Cardiolipin's propensity for phase transition and its reorganization by dynamin-related protein 1 form a basis for mitochondrial membrane fission

Natalia Stepanyants[a], Patrick J. Macdonald[a], Christopher A. Francy[b,c,d], Jason A. Mears[b,c,d], Xin Qi[a,b], and Rajesh Ramachandran[a,d]

[a]Department of Physiology and Biophysics, [b]Center for Mitochondrial Diseases, [c]Department of Pharmacology, and [d]Cleveland Center for Membrane and Structural Biology, Case Western Reserve University School of Medicine, Cleveland, OH 44106

ABSTRACT **Cardiolipin (CL) is an atypical, dimeric phospholipid essential for mitochondrial dynamics in eukaryotic cells. Dynamin-related protein 1 (Drp1), a cytosolic member of the dynamin superfamily of large GTPases, interacts with CL and functions to sustain the balance of mitochondrial division and fusion by catalyzing mitochondrial fission. Although recent studies have indicated a role for CL in stimulating Drp1 self-assembly and GTPase activity at the membrane surface, the mechanism by which CL functions in membrane fission, if at all, remains unclear. Here, using a variety of fluorescence spectroscopic and imaging approaches together with model membranes, we demonstrate that Drp1 and CL function cooperatively in effecting membrane constriction toward fission in three distinct steps. These involve 1) the preferential association of Drp1 with CL localized at a high spatial density in the membrane bilayer, 2) the reorganization of unconstrained, fluid-phase CL molecules in concert with Drp1 self-assembly, and 3) the increased propensity of CL to transition from a lamellar, bilayer arrangement to an inverted hexagonal, nonbilayer configuration in the presence of Drp1 and GTP, resulting in the creation of localized membrane constrictions that are primed for fission. Thus we propose that Drp1 and CL function in concert to catalyze mitochondrial division.**

Monitoring Editor
Patricia Bassereau
Institut Curie

Received: Jun 1, 2015
Revised: Jun 24, 2015
Accepted: Jul 1, 2015

This article was published online ahead of print in MBoC in Press (http://www.molbiolcell.org/cgi/doi/10.1091/mbc.E15-06-0330) on July 8, 2015.

Address correspondence to: Rajesh Ramachandran (rxr275@case.edu).

Abbreviations used: CL, cardiolipin; Dnm1p, dynamin-related protein 1 (in yeast); DOPA, dioleoylphosphatidic acid; DOPC, dioleoylphosphatidylcholine; DOPE, dioleoylphosphatidylethanolamine; DOPS, dioleoylphosphatidylserine; DPPC, dipalmitoylphosphatidylcholine; Drp1, dynamin-related protein1 (in mammals); Drp1-KO MEFs, Drp1-knockout mouse embryonic fibroblasts; DTT, dithiothreitol; ER, endoplasmic reticulum; FRET, Förster resonance energy transfer; GDP, guanosine diphosphate; GMP-PCP, β,γ-methyleneguanosine 5′-triphosphate; GTP, guanosine triphosphate; GUV, giant unilamellar vesicle; H_{II}, inverted hexagonal phase; l_d, liquid-disordered phase; l_o, liquid-ordered phase; LT, lipid nanotubes; Mff, mitochondrial fission factor; MIM, mitochondrial inner membrane; MOM, mitochondrial outer membrane; NBD-DHPE, *N*-(7-nitrobenz-2-oxa-1,3-diazol-4-yl)-1,2-dihexadecanoyl-*sn*-glycero-3-phosphoethanolamine; NBD-DOPE, 1,2-dioleoyl-*sn*-glycero-3-phosphoethanolamine-*N*-(7-nitro-2-1,3-benzoxadiazol-4-yl); $PI4,5P_2$, phosphatidylinositol-4,5-bisphosphate; POPC, 1-palmitoyl-2-oleoylphosphatidylcholine; Rh-DOPE, 1,2-dioleoyl-*sn*-glycero-3-phosphoethanolamine-*N*-(lissamine rhodamine B sulfonyl); TMCL, tetramyristoylcardiolipin; TopFluor-CL, 1,1′,2,2′-tetraoleoyl cardiolipin[4-(dipyrromethemeboron difluoride) butanoyl].

INTRODUCTION

Dynamin-superfamily GTPases catalyze multiple membrane remodeling events in the eukaryotic cell, including those of organellar division and fusion (Praefcke and McMahon, 2004; Heymann and Hinshaw, 2009). Dynamin-related protein 1 (Drp1), a cytosolic member of this extensive superfamily, establishes the critical balance of mitochondrial division and fusion by catalyzing mitochondrial membrane fission (Chan, 2012). In response to a variety of physiological cues, Drp1 translocates to the mitochondrial outer membrane (MOM) surface to initiate the membrane remodeling events that culminate in mitochondrial division. However, the molecular mechanisms underlying these processes are just beginning to be understood.

Unlike prototypical dynamin, Drp1 lacks an apparent lipid-binding domain and requires membrane-integrated adaptor proteins such as Fis1, Mff, and MiD49/51 for its recruitment to the MOM (Bui and Shaw, 2013; Labbe *et al*., 2014; Richter *et al*., 2015). However, we and others have recently identified the mitochondrion-specific lipid cardiolipin (CL) as a specific binding partner for Drp1 (Bustillo-Zabalbeitia *et al*., 2014; Macdonald *et al*., 2014; Ugarte-Uribe *et al*., 2014). CL facilitates the self-assembly of Drp1 into helical polymers

that tubulate membranes and also robustly stimulates Drp1 GTPase activity, two features considered functional hallmarks of these atypical GTPases (Heymann and Hinshaw, 2009). However, the nature of Drp1–CL interactions and the role of CL, if any, in the mitochondrial membrane–remodeling process remain unclear.

CL is an unusual dimeric phospholipid with unique biochemical and biophysical properties (Schlame *et al.*, 2005; Huang and Ramamurthi, 2010). Containing four predominantly linoleoyl (C18:2) acyl chains in higher eukaryotes, native CL has a small headgroup cross-sectional area and volume relative to its acyl chains, rendering it effectively cone shaped. Consequently, CL exhibits complex phase behavior in membranes, with a propensity to stabilize negative membrane curvature upon sequestration and to transition from a lamellar, bilayer phase to the nonlamellar, inverted hexagonal (H_{II}) configuration upon further enrichment (de Kruijff and Cullis, 1980; Seddon, 1990; Tarahovsky *et al.*, 2000; Trusova *et al.*, 2010; Renner and Weibel, 2011). This property of CL may be relevant to lipid rearrangement events that precipitate membrane fission or fusion, especially when considered in the context of mitochondrial membrane dynamics (Chernomordik and Kozlov, 2008; Doan *et al.*, 2013; Pan *et al.*, 2014). Indeed, the mitochondrial inner membrane (MIM) dynamin-related GTPase OPA1 depends critically on CL for promoting mitochondrial membrane fusion (DeVay *et al.*, 2009; Ban *et al.*, 2010). Furthermore, defects in the acyl chain remodeling of CL and the resultant variations in CL acyl chain composition lead to the cardioskeletal myopathy Barth syndrome, underlining the importance of this atypical lipid to proper mitochondrial function (Schlame and Ren, 2006). How Drp1 and CL function cooperatively in effecting mitochondrial membrane remodeling and fission remains unknown.

In this study, we demonstrate that Drp1 stably associates with CL localized at a high spatial density in the target lipid bilayer. We further show that Drp1 preferentially reorganizes unconstrained (i.e., non–raft-associated) fluid-phase CL to generate condensed membrane platforms for subsequent membrane remodeling. Stimulated GTP hydrolysis upon helical self-assembly induces further CL rearrangement, which appears to increase the propensity of the lipid to undergo a localized lamellar-to-nonlamellar phase transition. These CL rearrangements, dependent on Drp1 B-insert–membrane interactions, create narrowly constricted membrane regions that are predisposed for fission. Thus Drp1 and CL function cooperatively in facilitating membrane remodeling and fission during mitochondrial division.

RESULTS

Drp1 remodels fluid-phase CL

We previously found that a high spatial density of CL (>10 mol% CL) is required for the effective self-assembly and stimulation of GTPase activity of Drp1 on synthetic liposomes composed of a ternary mixture of native CL, dioleoylphosphatidylethanolamine (DOPE), and dioleoylphosphatidylcholine (DOPC; Macdonald *et al.*, 2014). Consistent with this observation, in independent studies (Ugarte-Uribe *et al.*, 2014), despite discernible membrane recruitment, very little stimulation of GTPase activity was observed for Drp1 on MOM-like liposomes that contained ~4 mol% CL (8% by weight). By contrast, the yeast Drp1 homologue Dnm1p was found to be maximally stimulated on MOM-like liposomes composed of a variety of negatively charged phospholipids but containing only ~3 mol% CL (6% by weight; Lackner *et al.*, 2009). Because the overall CL content of the MOM rarely exceeds 10 mol% under homeostatic conditions (van Meer *et al.*, 2008; Horvath and Daum, 2013; Cosentino and Garcia-Saez, 2014), we first determined whether other negatively charged phospholipids function cooperatively with CL in stimulating Drp1 GTPase activity, as observed for yeast Dnm1p earlier. Surprisingly, under similar conditions (i.e., with only 3 mol% CL in MOM-like liposomes), human Drp1 was not stimulated (Figure 1A). However, when the CL content was increased to 10 mol%, MOM-like liposomes were significantly more potent than a ternary CL/DOPE/DOPC mixture in stimulating Drp1 GTPase activity (Figure 1B). These data suggested that other negatively charged phospholipids, when localized together with CL at a relatively high spatial density in the membrane bilayer, positively promote Drp1 recruitment and stimulation. In this context, we surmised that CL-enriched microdomains that putatively exist at contact sites between the MIM and MOM (Ardail *et al.*, 1990; Sorice *et al.*, 2009; Macdonald *et al.*, 2014) function as "recruitment platforms" to promote stable Drp1 association and self-assembly on the mitochondrial surface. Indeed, Drp1 has been found associated with detergent-insoluble, raft-like microdomains isolated from the mitochondria of mammalian cells upon apoptotic stimulation of fission, suggesting that these sites correspond to sites of mitochondrial division (Ciarlo *et al.*, 2010; Sorice *et al.*, 2012).

Of interest, endoplasmic reticulum (ER)–mitochondria contact sites also mark locations of ensuing mitochondrial division and are enriched in cholesterol, which presumably promotes the formation of raft-like microdomains at these regions (Sorice *et al.*, 2009; Hayashi and Fujimoto, 2010; Friedman *et al.*, 2011; Arasaki *et al.*, 2015). Cholesterol does so by effecting exclusive and strong packing interactions between its hydrophobic core moieties and the saturated acyl chains of phospholipids, thereby facilitating membrane phase separation (Marsh, 2009). To determine whether the presence of cholesterol influences Drp1 recruitment to CL-containing membranes, we monitored Drp1 GTPase activity on liposomes containing a limiting concentration of native CL (10 mol%) but included a raft-promoting mixture of 1,2-dipalmitoylphosphatidylcholine (DPPC; C16:0-C16:0; 37.5 mol%) and cholesterol (25 mol%; Veatch and Keller, 2003; Beales *et al.*, 2011). DPPC accounts for almost one-third of the total PC species found in the mitochondria of specific mammalian tissues (Schlame *et al.*, 1988). Remarkably, a 10 mol% native CL–containing lipid mixture that included DPPC and cholesterol was significantly more effective than an equivalent CL-containing mixture containing only cholesterol in stimulating Drp1 GTPase activity (Figure 1C). When DPPC was replaced by 1-palmitoyl-2-oleoylphosphatidylcholine (POPC; C16:0-C18:1), which can still associate with cholesterol via its single, saturated acyl chain, albeit weakly compared with DPPC (de Almeida *et al.*, 2003; Marsh, 2009), the POPC- and cholesterol-containing lipid mixture was more effective than a corresponding mixture lacking cholesterol in stimulating Drp1 GTPase activity at a threshold CL concentration of 15 mol% (Figure 1D). Together these data established that the presence of raft-like microdomains in the lipid microenvironment of Drp1 drastically reduces the CL requirement for Drp1 self-assembly and GTPase stimulation, effectively approaching physiological CL levels.

Native CL, however, bears predominantly unsaturated acyl chains ($(C18:2)_4$) and is therefore expected to be excluded from condensed-phase lipid rafts (Schlame *et al.*, 2005; Beales *et al.*, 2011). Cholesterol could function to reduce the CL requirement of Drp1 via an "exclusion-based mechanism," that is, by enriching native CL, indirectly, in the non-raft, fluid-phase regions of the target membrane. Using a system of surface-immobilized giant unilamellar vesicles (GUVs) and confocal fluorescence microscopy as previously (Macdonald *et al.*, 2014), we sought direct visual evidence for this scenario. Because a mixture containing POPC and cholesterol is

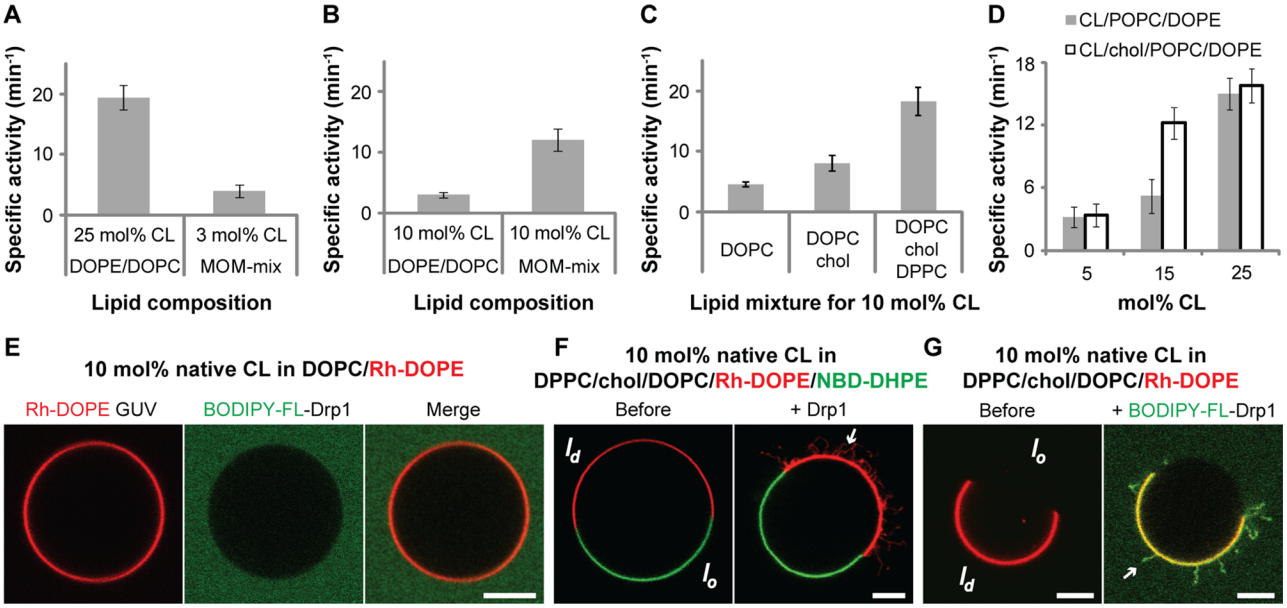

FIGURE 1: Drp1 preferentially remodels membranes containing a high spatial density of fluid-phase CL. (A–D) Stimulated GTPase activity of Drp1 WT (0.5 μM final) preassembled on liposomes of defined lipid composition (150 μM total lipid) containing varying mole fractions (mol%) of native CL plotted as specific activity (min^{-1}) ± SD ($n = 3$). (E) Confocal fluorescence images of surface-immobilized Rh-DOPE–labeled GUVs containing 10 mol% native CL (red; left) in the presence of BODIPY-FL-labeled Drp1 WT (0.5 μM protein final; green; middle). Right, merged images. (F) Confocal fluorescence images of GUVs phase-separated into raft-phase, liquid-ordered (l_o, NBD-DHPE–labeled, green), and fluid-phase, liquid-disordered (l_d, Rh-DOPE–labeled, red) membrane regions before (left) and after (right) addition of unlabeled Drp1 WT (0.5 μM final). Only merged images are shown. Arrow points to Drp1-generated membrane tubules originated from Rh-DOPE–labeled, fluid-phase membrane regions. (G) Same as F, but containing unlabeled, dark, raft-phase l_o regions before (left) and after (right) addition of BODIPY-FL–labeled Drp1 WT. Arrow points to Drp1-decorated membrane tubules originating from fluid-phase membrane regions. Only merged images are shown. Scale bar, 5 μm.

incapable of constituting sufficiently large lipid microdomains that can be resolved by light microscopy (typically less than ~300 nm; Marsh, 2009), we used a mixture containing DPPC and cholesterol that instead forms large micrometer-scale, phase-separated lipid microdomains that can be visualized easily (Beales *et al.*, 2011). As previously established (Beales *et al.*, 2011), we used *N*-(7-nitrobenz-2-oxa-1,3-diazol-4-yl)-1,2-dihexadecanoyl-*sn*-glycero-3-phosphoethanolamine (triethylammonium salt; NBD-DHPE) containing saturated acyl chains (0.5 mol%) and Rh-DOPE containing unsaturated acyl chains (0.1 mol%), respectively, as fluorescent lipid markers for the raft-like, liquid-ordered (liquid-condensed; l_o) and the fluid-like, liquid-disordered (liquid-expanded; l_d) regions of the membrane. In control experiments with Rh-DOPE–labeled GUVs (red) composed of a homogeneously fluid mixture of DOPC (90 mol%) and a limiting concentration of native CL (10 mol%), no stable membrane recruitment of Drp1 (BODIPY-FL–labeled Drp1; green) was observed (Figure 1E). However, when this lipid mixture was phase separated into l_o (NBD-DHPE–labeled; green) and l_d (Rh-DOPE–labeled; red) membrane regions via the inclusion of DPPC and cholesterol (Figure 1F, left), a selective recruitment of unlabeled Drp1 onto the fluid-phase regions of the membrane was observed, resulting in extensive membrane tubulation (Figure 1F, right). Two-color experiments with BODIPY-FL–labeled Drp1 and Rh-DOPE–labeled l_d regions of the membrane essentially confirmed this scenario (Figure 1G and Supplemental Movie S1). We conclude that the exclusion of native CL from raft-like lipid microdomains effectively increases its local concentration in the vicinity, that is, in the surrounding l_d regions of the membrane, to >10 mol% to promote Drp1 recruitment. Together these data suggested that the high spatial density of CL necessary for stable Drp1 recruitment and GTPase activation at membrane "contact sites" is achieved, not through the formation of CL-enriched rafts, but through its enrichment via raft exclusion. Of interest, nearly identical results have been obtained for cytochrome c–CL interactions (Beales *et al.*, 2011).

Drp1 associates with, but does not remodel, CL restricted to rafts

In yeast as well as in mammalian cells, the unsaturated acyl chains of native, mature CL ($(C18:2)_4$-CL in mammals) are generated from an enzymatic transacylation reaction involving immature, precursor CL species (e.g., monolysocardiolipin) as acceptor substrates (Baile *et al.*, 2014; Xu and Schlame, 2014). Mutations in the gene encoding for the CL transacylase tafazzin have been linked to the X-linked disease Barth syndrome, characterized by the accumulation of CL variants that carry a high proportion of saturated acyl chains (Schlame *et al.*, 2002, 2005). Because CL variants containing saturated acyl chains, unlike native CL, can favorably partition into raft-like lipid microdomains, we surmised that the presence of saturated CL at relatively high concentrations in the lipid bilayer could differentially affect Drp1 membrane recruitment and activity.

Moreover, because cholesterol is only poorly enriched at the MOM at concentrations ≤10 mol% (van Meer *et al.*, 2008; Horvath and Daum, 2013), we tested the raft-exclusion hypothesis directly by substituting cholesterol with a variant of CL, tetramyristoylcardiolipin (TMCL; $(C14:0)_4$), which contains saturated acyl chains at all four positions. TMCL behaves similarly to cholesterol and was previously shown to form condensed complexes or microdomains, either by itself or in association with other phospholipid molecules

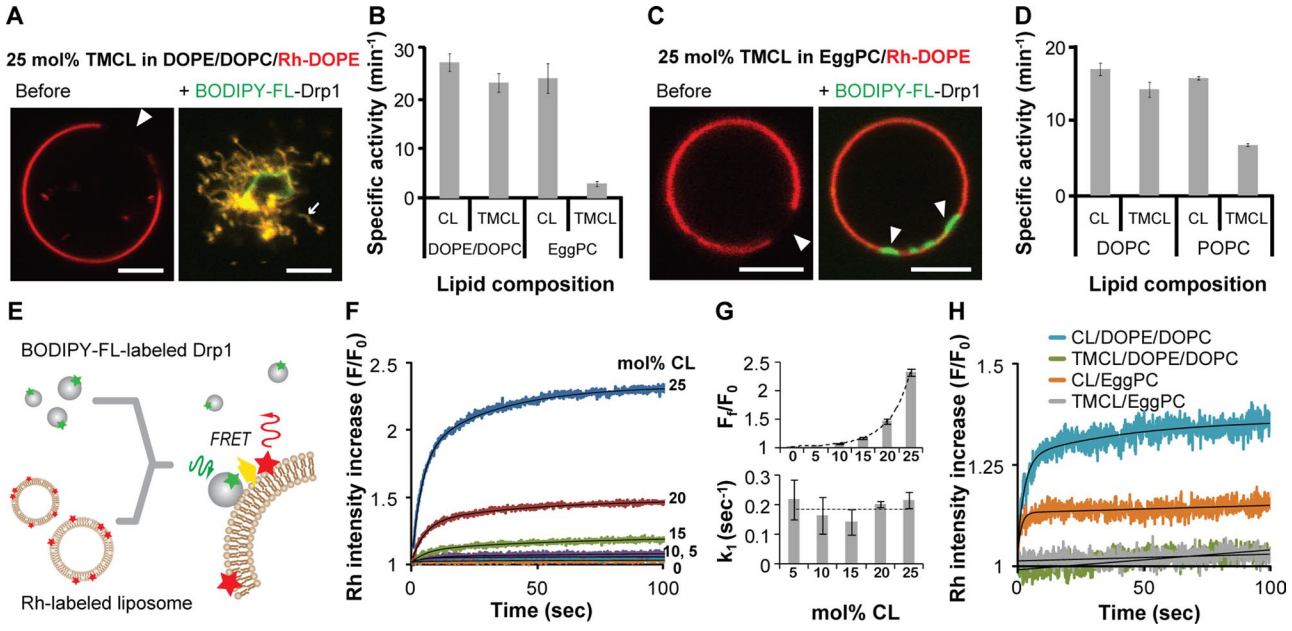

FIGURE 2: Drp1 does not remodel membranes containing constrained, raft-phase CL. (A) Confocal fluorescence images of phase-separated, TMCL-containing GUVs containing coexisting Rh-DOPE–labeled fluid (red) and unlabeled, raft-like (dark; arrow) membrane regions before (left) and after (right) addition of BODIPY-FL–labeled Drp1 WT (0.5 μM protein final). (B) Stimulated GTPase activity of Drp1 WT (0.5 μM final) preassembled on liposomes of defined lipid composition containing 25 mol% of either native CL or TMCL (150 μM total lipid) plotted as specific activity (min^{-1}) ± SD ($n = 3$). (C) Same as A, but with EggPC replacing both DOPC and DOPE. (D) Same as B, but on liposomes composed of a binary mixture of either DOPC or POPC and native CL or TMCL (25 mol% CL species) as indicated. (E) Schematic illustration of BODIPY-FL–Drp1–Rh-DOPE FRET on liposomes. (F) FRET-sensitized increase in rhodamine emission intensity as a function of CL concentration (in mol%) plotted as F/F_0, where F_0 and F represent the initial and at-time-t rhodamine emission intensities upon BODIPY–FL-Drp1 WT (0.1 μM final) addition to Rh-DOPE–labeled liposomes (10 μM total lipid). (G) The final extents (top) and the initial rates (bottom) of the FRET-sensitized rhodamine emission intensity increase upon stable BODIPY-FL–labeled Drp1 WT association plotted as a function of CL concentration. F_f represents the final emission intensity, and k_1 represents the major, apparent rate constant for the emission intensity increase. (H) FRET-sensitized increase in rhodamine emission intensity upon BODIPY-FL–Drp1 WT addition to TMCL- or native-CL–containing liposomes plotted as in G. Buffer contained 2 mM $MgCl_2$, which markedly reduces the affinity of Drp1 for CL-containing membranes as described in *Materials and Methods*. Scale bar, 5 μm.

that bear saturated acyl chains (Lewis and McElhaney, 2009; Maniti *et al.*, 2011; Boscia *et al.*, 2014). Indeed, in GUVs composed largely of unsaturated DOPC and DOPE but containing 25 mol% TMCL, lipid phase separation was clearly evident, as visualized by the demarcation of Rh-DOPE–labeled (red), fluid-phase regions of the membrane from unlabeled, dark, condensed-phase regions (Figure 2A, left). Remarkably, however, the dark regions rapidly dissipated upon BODIPY-FL–labeled Drp1 (green) recruitment, giving rise to Drp1-decorated membrane tubules that appeared to originate from the entire GUV surface (Figure 2A, right). These data indicated that Drp1 recognizes as well as reorganizes TMCL contained in microdomains when the saturated CL variant is present alongside highly fluid, unsaturated phospholipids that permit its reorganization. Furthermore, in the presence of DOPC and DOPE, TMCL was equivalent to native CL in stimulating Drp1 GTPase activity (Figure 2B), indicating that the presence of saturated acyl chains in CL does not deter either Drp1 membrane recruitment or self-assembly. On the contrary, when egg PC (predominantly POPC), which permits phospholipid acyl chain condensation, was substituted for DOPC and DOPE, TMCL, despite being able to recruit Drp1 to the membrane, did not permit any membrane remodeling (Figure 2C). Consistently, TMCL-containing liposomes were significantly inhibited in stimulating Drp1 GTPase activity under these specific conditions (Figure 2B). A similar inhibition was also observed for TMCL in the context of synthetic POPC when compared with DOPC (Figure 2D). These data conclusively demonstrate that CL-enriched rafts composed of condensed complexes of CL (here, TMCL) in association with other saturated phospholipids fail to promote Drp1-mediated membrane remodeling.

To validate the foregoing conclusions, we developed and used a Förster resonance energy transfer (FRET)–based approach to measure Drp1–membrane interactions directly and quantitatively. BODIPY-FL–labeled Drp1 was used as a FRET donor for rhodamine-labeled acceptor phospholipid molecules (Rh-DOPE, reconstituted at 1 mol%) dispersed in the membrane bilayer (Figure 2E). The FRET-sensitized increase in rhodamine emission intensity upon BODIPY-FL excitation was monitored to detect Drp1–membrane association directly and as a function of increasing CL concentration.

Consistent with earlier results (Macdonald *et al.*, 2014), the extent of Drp1 binding to native CL-containing liposomes was critically dependent on CL spatial density (Figure 2F). Because CL is present at a vast molar excess over Drp1 in our experiments, if CL were to function solely as a receptor for Drp1 or as a ligand that binds to each Drp1 molecule in a specified stoichiometry, reducing the concentration of CL in the membrane should affect only the kinetics and not the extent of Drp1–membrane association. However, only differences in the extent and not the rate of Drp1–membrane association were observed as a function of CL concentration (Figure 2G),

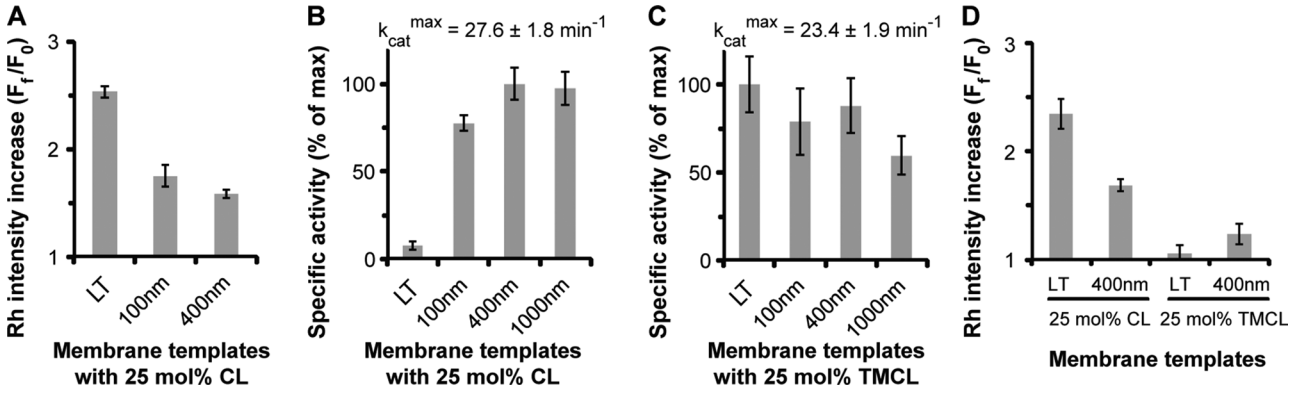

FIGURE 3: Membrane fluidity influences Drp1-induced CL reorganization. (A) Relative FRET-sensitized increase in Rh-DOPE emission intensity upon stable membrane association of BODIPY-FL–labeled Drp1 WT (0.1 μM final) on membrane templates of varying average diameter (liposomes) or fluidity (LTs; 10 μM total lipid) plotted as F_f/F_0, where F_f and F_0 represent the final and initial emission intensities, respectively. (B) Comparison of the stimulated GTPase activities of Drp1 WT (0.5 μM final) on the various membrane templates used (150 μM total lipid; $n = 3$). The data are plotted as percentage of maximum activity as indicated above. (C) Same as B, but with 25 mol% TMCL instead of native CL. (D) Same as A, but comparing native CL- and TMCL-containing membrane templates.

indicating that Drp1 recognizes a collective biochemical or biophysical feature of CL that is spatially enriched and unconstrained in the membrane bilayer. Of importance, no FRET was observed in TMCL-containing liposomes in the context of either DOPC/DOPE or egg PC lipid mixtures (Figure 2H). Whereas for egg PC, this is consistent with TMCL-containing condensed-phase rafts excluding unsaturated, fluid-phase Rh-DOPE molecules for efficient FRET in unremodeled liposomes, in the case of DOPE/DOPC, it is most likely due to the limited access of fluid Rh-DOPE molecules to TMCL-enriched condensed membrane regions localized directly underneath the helical Drp1 scaffold in Drp1-decorated membrane tubules.

To determine the role of membrane fluidity in the Drp1 CL recognition and reorganization, we compared the extent of Drp1–membrane association and GTPase stimulation on fluid-phase liposomes with that that on diffusion-limited, precurved lipid nanotubes (LTs; ~30 nm in diameter) containing the order-inducing sphingolipid, C24:1 β-D-galactosylceramide (Stowell *et al.*, 1999; Pinto *et al.*, 2008). We previously demonstrated that Drp1 forms helical polymers on LTs (Macdonald *et al.*, 2014). Despite a greater, FRET-detected extent of Drp1 association with native CL-containing LTs in comparison to liposomes (Figure 3A), very little stimulation of GTPase activity was observed for Drp1 on these highly curved membrane templates (Figure 3B). However, no such difference was observed between liposome preparations of varying average diameter, consistent with the curvature-adaptive nature of Drp1 polymerization (Figure 3B; Bustillo-Zabalbeitia *et al.*, 2014; Macdonald *et al.*, 2014; Ugarte-Uribe *et al.*, 2014; Francy *et al.*, 2015). We reasoned that the inefficacy of native CL in LTs to effectively stimulate Drp1 GTPase activity is likely a result of the inability of Drp1 to reorganize CL molecules within the ordered confines of this membrane template and to properly align its GTPase domains for maximal GTPase activation upon helical self-assembly. If true, the presence of preorganized, clustered CL might alleviate this defect. Indeed, when native CL in LTs was replaced by TMCL, which has a tendency to segregate on its own (Figure 2A), Drp1 GTPase stimulation was fully restored to match that on corresponding liposomes (Figure 3C). Thus the combined and synergistic effect of membrane curvature as well as of preclustered CL (TMCL) obviates the need for Drp1-induced CL reorganization in LTs to effect proper Drp1 self-assembly and GTPase stimulation. Formation of condensed TMCL membrane patches in LTs was confirmed, albeit indirectly, by the lack of FRET between BODIPY-FL–labeled Drp1 and Rh-DOPE molecules, which are excluded from these regions (Figure 3D).

Taken together, these data indicated that stable Drp1 binding to CL-containing membranes and its maximal GTPase stimulation require that the local CL concentration exceed a certain threshold and that the CL molecules not be tied up in condensed complexes or rafts in association with other phospholipid molecules in the lipid bilayer. We conclude that spatially enriched, unconstrained, fluid-phase CL molecules that can be readily reorganized in the membrane bilayer ably support stable Drp1–membrane association, self-assembly, and GTPase stimulation.

Drp1 induces formation of CL-containing, condensed membrane regions

Prototypical dynamin alters the local distribution of its target lipid, phosphatidyinositol-4,5-bisphosphate (PI4,5P_2), at the endocytic pit neck, using its pleckstrin homology (PH) domain (Bethoney *et al.*, 2009). Dynamin-induced PI4,5P_2 clustering and the resultant line tension between the PI4,5P_2-enriched membrane neck and the surrounding bulk lipids have been proposed to accelerate the formation of a "hemifission intermediate" that ultimately precipitates nonleaky membrane fission (Liu *et al.*, 2006).

To determine whether Drp1 facilitates such a reorganization of its lipid target, CL, at the MOM, we adopted a fluorescence-based experimental strategy previously used for dynamin and PI4,5P_2 (Bethoney *et al.*, 2009). Here we analyzed the ability of Drp1 to promote the proximity-induced self-quenching of lipid head-group, BODIPY-conjugated, TopFluor-CL molecules bearing unsaturated acyl chains that were incorporated at a low spatial density (1 mol%) in liposomes in the presence of a vast excess of unlabeled CL to support stable Drp1–membrane association. Drp1 wild type (WT) promoted the self-quenching of TopFluor-CL in a protein concentration–dependent manner, indicating that Drp1 induces CL clustering at a nanometer scale (Figure 4A). Much to our surprise, a Drp1 B-insert mutant with an apparently reduced binding affinity for CL-containing membranes, Drp1 4KA (K557A + K560A + K569A + K571A; Bustillo-Zabalbeitia *et al.*, 2014), and a deletion mutant, Drp1 ΔB (Δ514-602; Frohlich *et al.*, 2013), lacking this region in its entirety both induced a similar level of TopFluor-CL self-quenching

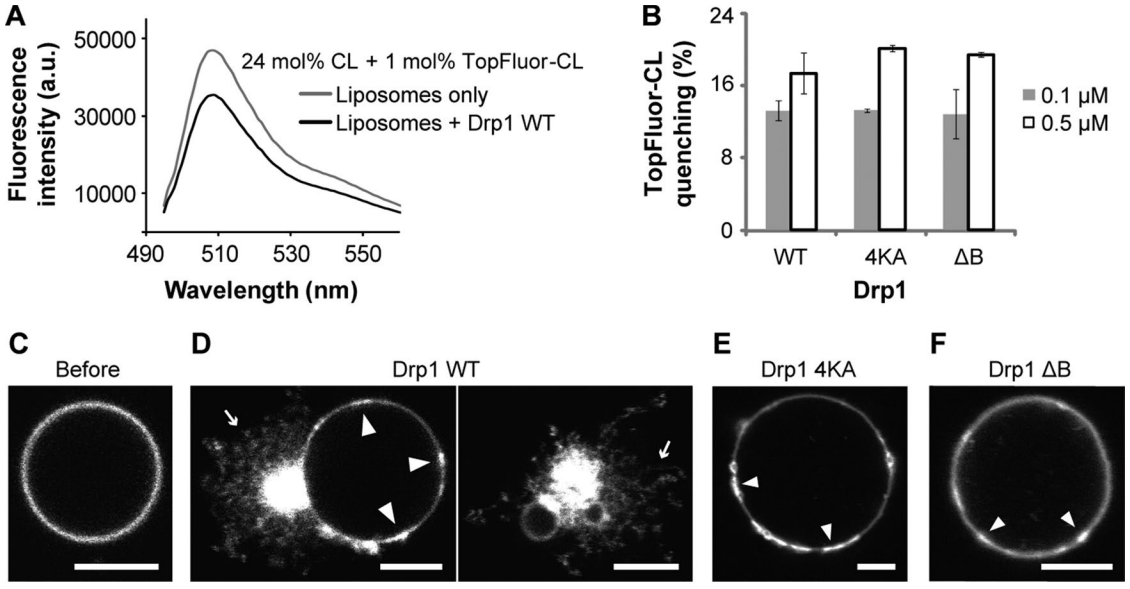

FIGURE 4: Drp1 reorganizes CL into condensed membrane regions. (A) Emission spectra of TopFluor-CL in native CL-containing liposomes (150 μM total lipid) before and after addition of Drp1 WT (0.5 μM final). (B) Extent of TopFluor-CL self-quenching as a function of Drp1 WT or mutant concentration is plotted as percent quenching. (C–F) Confocal fluorescence images of TopFluor-CL distribution in GUVs before (C) and after addition of 0.5 μM (final) Drp1 WT (D) or mutants (E, F). Slender arrows point to membrane tubules, and block arrows point to highly intense, condensed membrane regions. Scale bar, 5 μm.

(Figure 4B). Extensive biochemical and biophysical analyses revealed a self-assembly defect for these mutants on CL-containing membranes that consequently also abrogated membrane tubulation (Supplemental Figure S1, A–D). These data suggested that transient Drp1–membrane interactions, even in the absence of helical Drp1 self-assembly, sufficiently induce local CL reorganization in the membrane bilayer.

To determine whether Drp1 promotes the formation of CL clusters on a larger, micrometer scale as demonstrated recently for BAR (Bin-Amphiphysin-Rvs) domain–containing proteins and $PI4,5P_2$ (Zhao *et al.*, 2013), we used GUVs and confocal fluorescence microscopy to visualize potential changes in TopFluor-CL distribution as a consequence of Drp1–membrane interactions. In addition to promoting extensive membrane tubulation, Drp1 WT also induced the formation of regions of high TopFluor-CL intensity on the GUV surface (Figure 4, C and D). Unlike the case for BAR proteins (Zhao *et al.*, 2013), however, these membrane regions were not exclusively enriched in CL, as zwitterionic Rh-DOPE representing bulk-phase lipids in the bilayer was also highly intense. These data suggested that Drp1 induces the formation of what we refer to as "condensed membrane platforms" characterized by a higher spatial density of lipids present relative to the rest of the GUV membrane surface. Control experiments with self-assembly–defective Drp1 4KA revealed that these condensed membrane platforms formed upon initial Drp1–membrane contact before helical Drp1 self-assembly (Figure 4E and Supplemental Figure S1, E and F). Collectively these data revealed the existence of two distinct steps of Drp1–CL interaction that presumably operate in tandem before Drp1-mediated membrane tubulation. The first step involves the nanometer-scale clustering of CL induced by transient Drp1–membrane interaction, and the second step is the subsequent coalescence of these nanometer-scale clusters to form micrometer-scale condensed membrane regions.

Pointing to a role for the Drp1 B-insert in the latter step, the extent of membrane condensation induced by Drp1 ΔB was relatively minor compared with Drp1 4KA (Figure 4F and Supplemental Figure S1, E and F). In light of Drp1 ΔB's ability to promote the nanometer-scale clustering of CL in equal measure to Drp1 WT (Figure 4B), we suggest that the Drp1 B-insert, besides regulating Drp1 self-assembly (Strack and Cribbs, 2012; Frohlich *et al.*, 2013; Francy *et al.*, 2015), functions to assimilate the locally clustered CL molecules induced by transient Drp1–membrane interactions and stabilize their presence in the condensed membrane regions upon stable membrane association. We propose that the Drp1 B-insert region thus functions to induce the formation of CL-containing condensed membrane platforms in mitochondrial membranes.

Drp1 enhances CL phase transition propensity dependent on B-insert and bound nucleotide

Given that CL rapidly undergoes a phase transition from a lamellar, bilayer arrangement to the nonlamellar, H_{II} configuration upon enrichment (de Kruijff and Cullis, 1980; Seddon, 1990; Tarahovsky *et al.*, 2000; Trusova *et al.*, 2010; Renner and Weibel, 2011), we further investigated the effect of Drp1 on membrane phase behavior. To this end, we used a well-established, thoroughly validated fluorescence spectroscopic assay to monitor the potential Drp1-induced lamellar-to-H_{II} membrane phase transition in our CL-containing lipid bilayers (Hong *et al.*, 1988; Ortiz *et al.*, 1999). In this assay, head-group–modified NBD-DOPE molecules incorporated at 0.2 mol% in CL-containing lipid bilayers experience a dramatic increase in NBD emission intensity upon membrane phase transition from a lamellar, bilayer phase to the nonlamellar, H_{II} phase. In validation experiments, addition of calcium (Ca^{2+}) ions (5–25 mM $CaCl_2$) to native CL-containing liposomes induced a pronounced and concentration-dependent increase in NBD emission intensity, consistent with the established ability of divalent cations to promote the lamellar-to-H_{II} phase transition (Supplemental Figure S2A; Hong *et al.*, 1988; Tarahovsky *et al.*, 2000). Moreover, the observed changes were dependent also on the presence of DOPE, another cone-shaped, but zwitterionic, lipid with a similar propensity to undergo the lamellar-to-H_{II} phase transition at high local

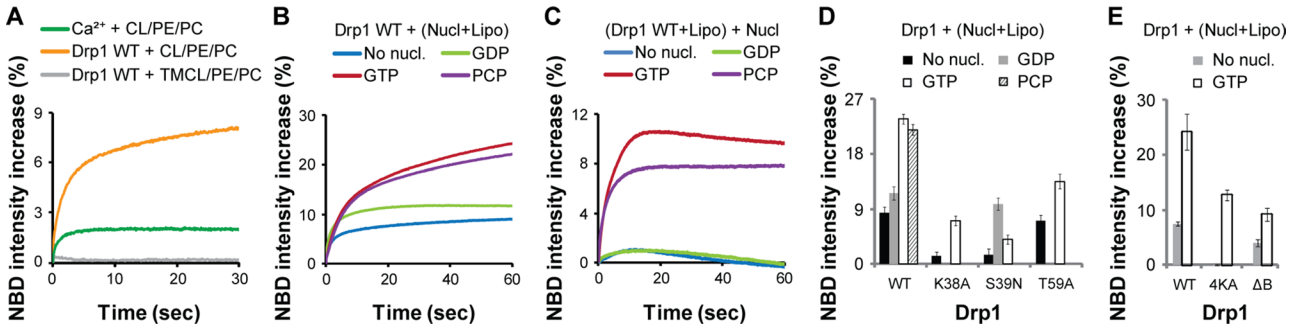

FIGURE 5: Drp1 induces apparent GTP- and B-insert–dependent CL phase transition. (A) NBD emission intensity change in liposomes containing either 25 mol% native CL or TMCL in the presence of DOPC and DOPE (50 μM total lipid) upon addition of Drp1 WT (0.5 μM final). Relative extent of lamellar-to-H_{II} membrane phase transition induced by Ca^{2+} ions (5 mM $CaCl_2$ final; Supplemental Figure S2A) is shown for comparison. (B) NBD emission intensity change upon addition of Drp1 WT (0.5 μM final) to 25 mol% native CL-containing liposomes (50 μM total lipid) in the constant presence of various nucleotides (nucl; 1 mM final). (C) NBD emission intensity increase upon addition of various nucleotides (1 mM final) to Drp1 WT (0.5 μM final) preassembled on 25 mol% native CL-containing liposomes (50 μM total lipid) before nucleotide addition. (D, E) Comparison of the extent of NBD emission intensity increase observed for Drp1 WT on 25 mol% native CL-containing liposomes (Lipo) in the constant presence of nucleotides as in B with that of GTPase domain mutants (D) or B-insert mutants (E).

concentrations (Supplemental Figure S2B; Hong *et al.*, 1988; Tarahovsky *et al.*, 2000).

Addition of Drp1 WT (0.5 μM final) to native CL-containing liposomes, in comparison to 5 mM $CaCl_2$, elicited a much greater NBD emission intensity increase, indicating a substantial propensity for phase transition induced by Drp1–CL interactions (Figure 5A). Moreover, as in the case of calcium ions, the apparent Drp1-induced membrane phase transition was significantly enhanced by the presence of DOPE (Supplemental Figure S2C). By contrast, no such increase was observed for TMCL-containing liposomes (Figure 5A), even when DOPE was present. This is consistent with the previously established inability of saturated, constrained TMCL molecules to undergo the lamellar-to-H_{II} phase transition (Sankaram *et al.*, 1989), despite being able to bind Drp1, and support Drp1-mediated membrane tubulation in the presence of unsaturated lipids (Figure 2A). The initial fluorescence intensity (F_0) of NBD-DOPE incorporated in TMCL-containing liposomes (8.7 ± 1.1 detector volts) was comparable to that of NBD-DOPE in native CL-containing liposomes (8.2 ± 0.3 detector volts), indicating that the unsaturated NBD-DOPE molecules were not preclustered or sequestered in TMCL-containing liposomes. Thus TMCL served as an ideal control for monitoring the Drp1-induced apparent membrane phase transition, as well as for visualizing the consequent membrane morphological changes (see later discussion), in native CL-containing membranes.

To assess the effect of nucleotide on the Drp1-induced CL phase transition, we monitored the extent of NBD emission intensity change in the constant presence of various nucleotides. Remarkably, Drp1 WT elicited a significantly greater NBD emission intensity increase in the presence of GTP or of its nonhydrolyzable analogue GMP-PCP than in the presence of GDP or in the absence of nucleotide (Figure 5B). Consistent with this observation, when Drp1 was preassembled onto liposomes before nucleotide addition, only the addition of GTP or GMP-PCP elicited a further NBD emission intensity increase (Figure 5C). These data indicated that Drp1 enhances CL phase transition propensity in a nucleotide-dependent manner.

To resolve the role of GTP binding versus hydrolysis in the apparent CL phase transition, we used well-known Drp1 GTPase domain mutants Drp1 K38A, Drp1 S39N, and Drp1 T59A as controls. Although all three mutants are defective in GTP hydrolysis, they remain trapped at different stages of the GTP hydrolysis cycle (Naylor *et al.*, 2006; Lackner *et al.*, 2009). Whereas Drp1 K38A (equivalent to dynamin 1 K44A and Dnm1p K41A) and Drp1 T59A (equivalent to dynamin 1 T65A) both bind GTP, albeit weakly in comparison to Drp1 WT (Warnock *et al.*, 1996; Song *et al.*, 2004; Naylor *et al.*, 2006), Drp1 S39N (equivalent to dynamin 1 S45N) preferentially binds GDP but not GTP (Marks *et al.*, 2001; Naylor *et al.*, 2006).

For reasons yet unclear, with the exception of Drp1 T59A, the NBD emission intensity increase observed for the mutants in the absence of nucleotide was considerably lower than that of wild type (Figure 5D). However, in the presence of GTP, key differences emerged. Consistent with their reduced GTP-binding affinities, the NBD emission intensity increase observed for Drp1 K38A and Drp1 T59A was substantially lower than that of Drp1 WT, even though Drp1 T59A, as earlier, fared marginally better in comparison to Drp1 K38A (Figure 5D). On the other hand, Drp1 S39N responded partially only to GDP but not to GTP (Figure 5D). On the basis of these data, we conclude that GTP binding–dependent conformational changes in Drp1 favorably promote CL phase transition propensity.

To determine a role for the Drp1 B-insert in this process, we examined NBD emission intensity changes in the presence of Drp1 B-insert mutants Drp1 4KA and Drp1 ΔB. The B-insert region of Drp1 has been implicated in effecting specific CL interactions (Bustillo-Zabalbeitia *et al.*, 2014). Consistent with this role, the NBD emission intensity increase observed for the mutants either in the presence or in absence of GTP was significantly lower than that of Drp1 WT (Figure 5E). These data indicated that the Drp1 B-insert region plays an important role in the apparent GTP-dependent CL phase transition.

GTP hydrolysis–dependent CL reorganization causes local membrane constriction

Because GTP hydrolysis in Drp1 is required for membrane fission, we sought to unravel the differential roles of GTP binding and GTP hydrolysis, if any, in Drp1-dependent membrane remodeling. To this end, we visualized the effects of GTP binding and hydrolysis and the resultant enhancement in CL phase transition on GUV membrane

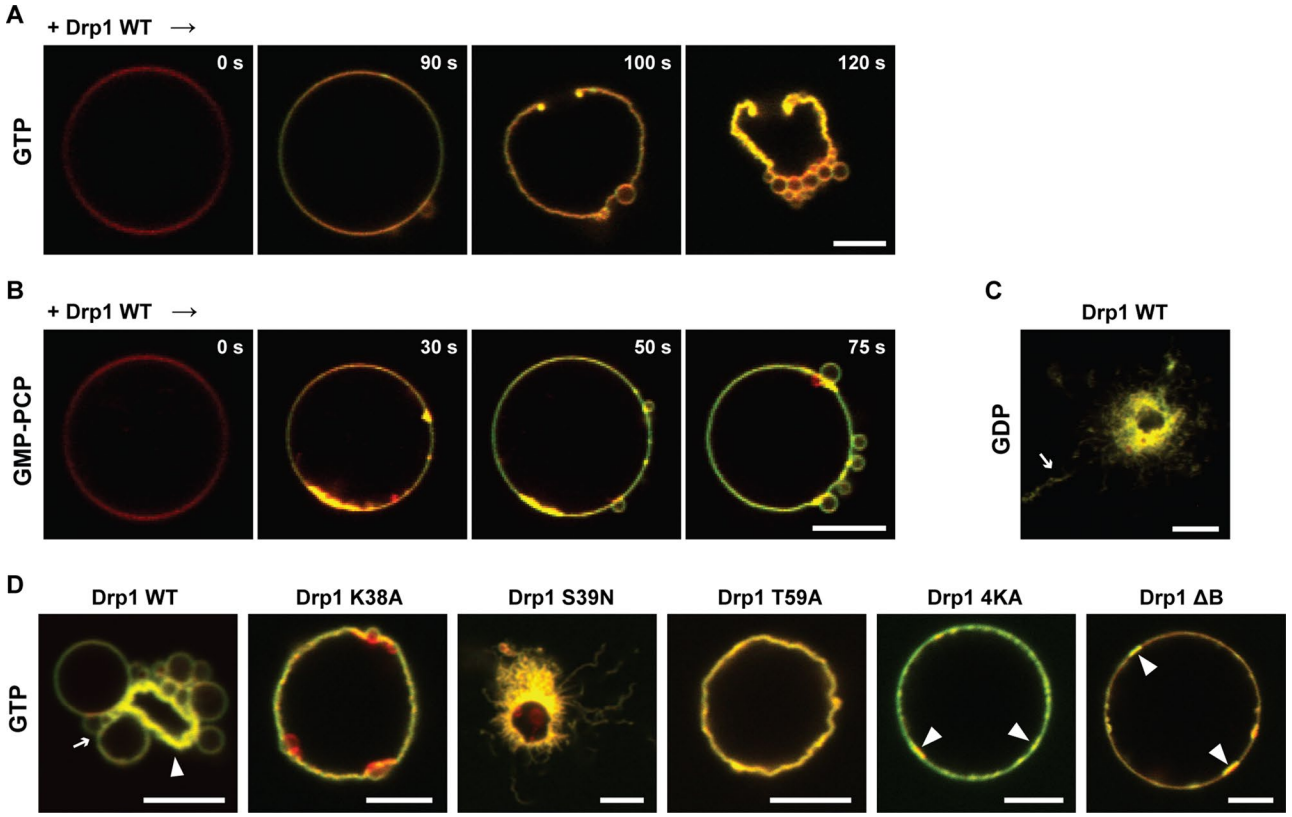

FIGURE 6: GTP-dependent apparent CL phase transition causes membrane constriction. (A) Time course of Rh-DOPE–labeled GUV membrane morphology changes upon BODIPY-FL–labeled Drp1 WT (0.5 μM final) addition in the constant presence of GTP (1 mM). (B) Same as A, but in the constant presence of GMP-PCP. (C) Endpoint confocal fluorescence image of Drp1 WT-induced GUV membrane remodeling as before but in the constant presence of GDP. (D) same as C, but for various Drp1 mutants in the constant presence of GTP. Slender arrow in C points to Drp1-decorated membrane tubules. In the D panels, slender arrows point to constricted "membrane buds," whereas triangular, block arrows point to condensed regions of the membrane that presumably mark sites of extensive CL lamellar-to-H_{II} phase transition. Scale bar, 5 μm.

morphology. Drp1 WT, unlike in the absence of nucleotide (Figure 4D), did not tubulate GUVs in the constant presence of GTP. Instead, Drp1 (0.5 μM final) initiated a series of membrane-remodeling events consistent with the enhanced lamellar-to-H_{II} membrane phase transition (Figure 6A and Supplemental Movie S2). These events ensued with the formation of condensed membrane regions on the GUV surface consistent with the initial Drp1-induced CL reorganization (Figure 4B). This was accompanied by significant membrane ruffling, resulting often in the loss of vesicle bilayer integrity via the formation of membrane pores. The process culminated in the creation of numerous constricted membrane regions on the GUV surface that pinched the vesicle into a series of membrane buds (Figure 6A and Supplemental Movie S2). The constricted membrane buds, however, remained tethered to the parent GUV membrane without undergoing fission. By contrast, no membrane deformation was evident for TMCL-containing GUVs despite the apparent, partial TMCL redistribution away from rafts to the rest of the fluid membrane induced by Drp1 in the constant presence of GTP (Supplemental Figure S3A and Figure 2A). These results were again consistent with the inability of TMCL molecules to undergo the lamellar-to-H_{II} phase transition despite being able to be reorganized by Drp1 either in the presence (Supplemental Figure S3A) or absence of GTP (Figure 2A). For native CL-containing GUVs, the extent of GUV membrane remodeling observed in the constant presence of GTP was proportional to Drp1 concentration (Supplemental Figure S3B). Of importance, at limiting concentrations (0.1 μM final), Drp1 induced the formation of membrane buds on the GUV surface without compromising vesicle integrity (Supplemental Figure S3B). These data confirmed that the creation of pores on the GUV surface (Figure 6A) is not a prerequisite for, and is unrelated to, the observed membrane constriction and budding.

In the presence of GMP-PCP, the GUVs remained largely intact, with only a relatively small proportion of buds formed on the membrane surface compared with GTP (Figure 6B and Supplemental Movie S3). In the presence of GDP, as in the absence of nucleotide, mostly membrane tubulation was observed (Figure 6C). The lack of significant membrane constriction and budding in the presence of GMP-PCP likely reflects the dynamic equilibrium that exists between the distinct in-solution and membrane-bound oligomeric forms of Drp1, as established previously (Macdonald *et al.*, 2014). The formation of a significant fraction of in-solution polymers of Drp1 in the presence of GMP-PCP might limit the availability of soluble Drp1 dimers required for nucleating helical polymerization on membranes. On the other hand, GTP hydrolysis, by reversing Drp1 higher-order polymerization in solution (Macdonald *et al.*, 2014), as well as by promoting the cyclical assembly and disassembly of Drp1 on membranes (Mears *et al.*, 2011; Francy *et al.*, 2015), enhances membrane constriction by restricting Drp1 self-assembly to limited regions of the membrane surface. GTP and GMP-PCP thus, by eliciting distinct,

nucleotide-dependent rearrangements in Drp1, may give rise to similar membrane-remodeling events, albeit to varying extents.

It is important to note that the membrane shape transformations observed here were born of single, surface-immobilized GUVs. These results are in sharp contrast to early (Montessuit *et al.*, 2010) as well as more recent (Ugarte-Uribe *et al.*, 2014) observations of Drp1-mediated membrane remodeling, in which, based on its tendency to cluster freely suspended liposomes (or GUVs) in solution, Drp1 has been proposed to function in membrane fission by first tethering juxtaposed membrane surfaces and subsequently aiding the formation of a hemifused membrane intermediate. Although these observations, given the affinity of Drp1 to bind to and be activated by the fusogenic lipid phosphatidic acid (PA) (Macdonald *et al.*, 2014; Ugarte-Uribe *et al.*, 2014), may be relevant to membrane fusion or possibly to the stabilization of free mitochondrial membrane poles postfission, it is incompatible with the formation of a topological membrane intermediate en route to membrane fission.

Control experiments with various GTP hydrolysis–defective Drp1 mutants (Supplemental Figure S4, A and B) in the constant presence of GTP validated our conclusions (Figure 6D). Although Drp1 WT and Drp1 K38A both induced membrane constriction (budding), Drp1 WT, at the single-vesicle level, deformed GUVs more extensively than Drp1 K38A. These data correlated well with the differential extents of membrane CL phase transition observed for Drp1 WT and Drp1 K38A in the presence of GTP (Figure 5D). Of note, the extent of GUV membrane remodeling induced by Drp1 K38A in the presence of GTP was comparable at a morphological level to that of Drp1 WT in the presence of GMP-PCP (Figure 6, B and D). By contrast, Drp1 S39N, consistent with a GTP-binding defect, tubulated GUVs extensively and in an unregulated manner regardless of the nucleotide species present (Figure 6D and Supplemental Figure S4C).

Inexplicably, both Drp1 K38A and Drp1 T59A, unlike Drp1 WT and Drp1 S39N, failed to tubulate GUVs even in the absence of nucleotide and instead induced significant membrane condensation, ruffling, or constriction under all conditions tested (Supplemental Figure S4C). These data suggested that the initial, in-solution conformations (or oligomeric states) of these two mutants may be drastically different from that of Drp1 WT and that the mutants are likely trapped in a conformation that mimics the GTP-bound state of Drp1 WT even in the absence of GTP in solution. In partial support of this hypothesis, Drp1 K38A was observed previously to be aggregation-prone in solution (Ugarte-Uribe *et al.*, 2014). Furthermore, Drp1 K38A constituted a significant fraction of higher-order polymers even in the constant presence of GTP in solution, whereas GTP hydrolysis characteristically induced polymer disassembly in Drp1 WT (Supplemental Figure S4D). Drp1 S39N did not sediment variably under any condition tested (Supplemental Figure S4D).

Unlike the case of the GTPase-domain mutants, GUV shape transformations were barely discernible for the B-insert mutants Drp1 4KA and Drp1 ΔB, largely owing to their respective self-assembly and CL-interaction defects. On the basis of the collective data, we conclude that Drp1 constricts and remodels CL-containing membranes by inducing CL reorganization and membrane phase transition in a GTP hydrolysis–dependent manner.

Drp1-induced membrane constriction predisposes membrane for fission

Using time-lapse electron microscopy (EM), we sought direct structural evidence for the observed Drp1-induced CL reorganization and GTP-dependent membrane morphology changes and assessed their ramifications on membrane fission. Recent EM measurements revealed that Drp1 helices, preassembled on liposomes composed of a singular lipid (dioleoylphosphatidylserine [DOPS]), constrict the underlying lipid template further, both uniformly and contiguously, upon GTP hydrolysis (Koirala *et al.*, 2013; Francy *et al.*, 2015). Because GTP-dependent membrane morphology changes are readily assessed by EM under these conditions, we examined the structure of Drp1-decorated membrane tubules, at the onset of stimulated GTP hydrolysis, on CL-containing liposomes composed of a ternary mixture of native CL, DOPC, and DOPE. As expected, Drp1 induced the rapid constriction of these mixed-lipid membrane templates upon GTP hydrolysis (Figure 7A). Remarkably, however, in stark contrast to pure DOPS membranes (Koirala *et al.*, 2013; Francy *et al.*, 2015), Drp1 constricted the initial, uniformly diametric membrane tubules in a discontinuous manner, leading to the formation of highly localized and very narrowly pinched membrane regions (Figure 7A; arrows). Strikingly, these locally constricted membrane regions transformed the membrane tubules into a series of tethered membrane buds akin to a beads-on-a-string arrangement. This phenomenon was consistent with local CL reorganization, sequestration, and lipid demixing. Of importance, the membrane morphology changes induced by preassembled Drp1 upon GTP addition recapitulated results observed by confocal fluorescence microscopy in the constant presence of GTP (Figure 6A and Supplemental Figure S3B). Flanked by regions of high negative membrane curvature that possibly accommodates the conical shapes of CL and PE, these very narrowly constricted membrane regions (Figure 7A, right, inset), however, remained contiguous with the rest of the membrane tubule and presented no evidence of fission.

In control EM experiments with Drp1 and TMCL-containing liposomes, in the presence of GTP, no membrane remodeling was evident (Supplemental Figure S5A). This was again consistent with results obtained by fluorescence microscopy (Supplemental Figure S3A). Unlike GTP, the addition of GDP did not elicit any significant morphological change in Drp1-decorated membrane tubules (Supplemental Figure S5B). On the basis of these structural data, we conclude that Drp1, upon GTP hydrolysis, induces CL reorganization, generation of high negative membrane curvature, and local membrane constriction.

Drp1–CL interactions are essential for mitochondrial fission in vivo

To ascertain a role for Drp1–CL interactions in mitochondrial division in vivo, we tested the ability of CL interaction–defective Drp1 4KA to rescue the mitochondrial fission defect observed in Drp1-knockout (KO) cells (Macdonald *et al.*, 2014). Whereas Drp1 WT expression resulted in extensive mitochondrial fragmentation, Drp1 4KA expression resulted in the formation of hyperfused mitochondrial networks that were largely localized to the perinuclear region (Figure 7, B–D). From these data, we conclude that Drp1–CL interactions play a critical role in mitochondrial fission in vivo.

DISCUSSION

In the case of prototypical dynamin, lipid phase separation and the resultant line tension from the PH domain–mediated clustering of $PI4,5P_2$ molecules at the endocytic membrane neck have been proposed to facilitate membrane fission (Bethoney *et al.*, 2009). On the basis of our experimental data, we consider a similar scenario but one that instead involves a locally induced CL phase transition upon Drp1 activity as one of several possible mechanisms by which Drp1 catalyzes membrane fission (Figure 7E). The requirement of both

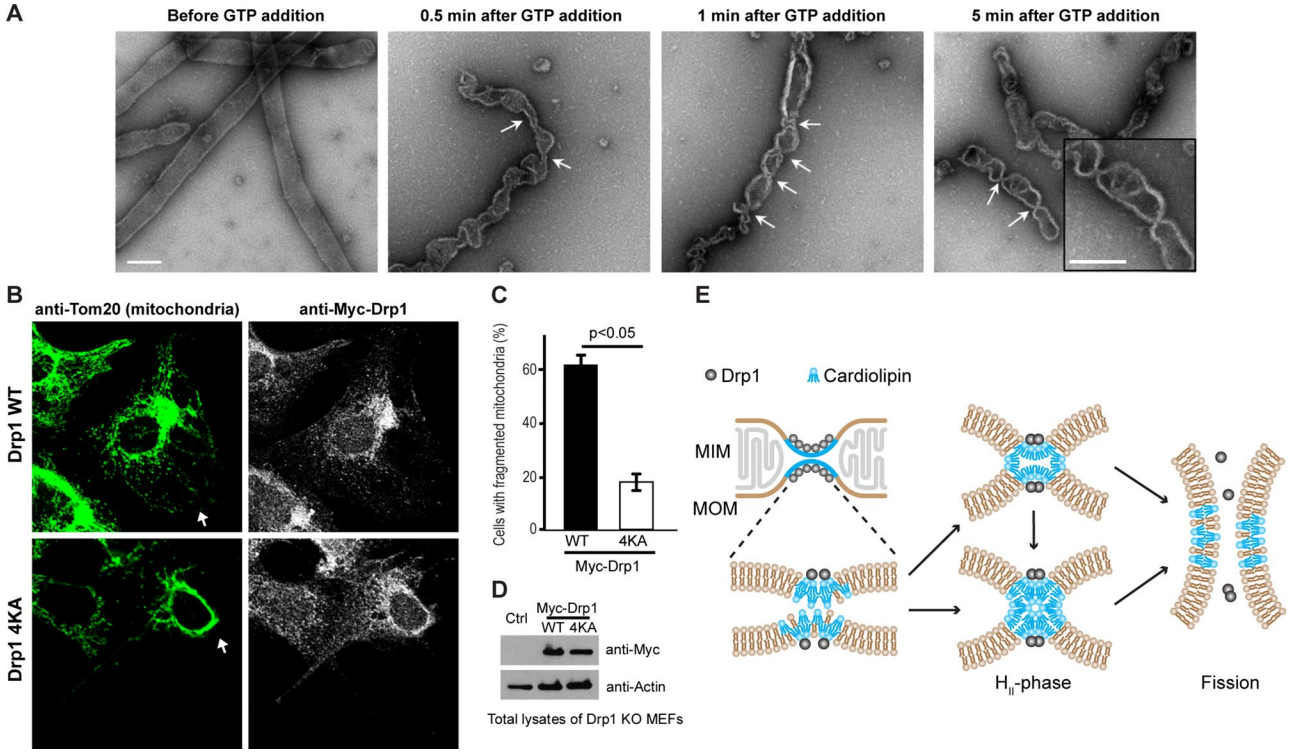

FIGURE 7: Drp1–CL interactions generate membrane constriction for fission both in vitro and in vivo. (A) Representative negative-stain EM images of Drp1-decorated membrane tubules displaying time-dependent membrane morphology changes upon GTP hydrolysis. Arrows point to highly localized, narrowly constricted regions of the membrane tubule that are predisposed to fission. Far right, inset, enlarged portion of the image. Scale bars, 200 nm. (B) Confocal fluorescence images of mitochondrial morphology (left; green) in Drp1 KO MEFs expressing either Myc-tagged Drp1 WT or Drp1 4KA (red; grayscaled for clarity; right). Arrows point to either fragmented mitochondria (in the case of Drp1 WT) or hyperfused mitochondrial networks (in the case of Drp1 4KA) localized to the perinuclear region of the cell. (C) Quantification of mitochondrial fragmentation in Drp1 KO MEFs cells expressing either Myc-tagged Drp1 WT or Drp1 4KA. (D) Representative Western blot showing expression levels of Myc-tagged Drp1 WT and Drp1 4KA in transfected Drp1 KO MEFs. Untransfected cells (Ctrl) served as negative control, and actin was used as loading control for total protein. (E) Model of Drp1-induced CL reorganization and phase transition at the MOM surface that presumably leads to membrane fission and mitochondrial division. H_{II} phase, inverted, hexagonal phase; MIM, mitochondrial inner membrane; MOM, mitochondrial outer membrane.

native CL and DOPE for the apparent membrane phase transition and for the formation of potential fission sites in vitro might explain why the combined loss of these two phospholipids is lethal in vivo (Gohil *et al.*, 2005). Our data also suggest that under conditions of limited CL availability, other negatively charged lipids, including PA, which also adopts a conical shape and prefers negative membrane curvature, compensate for CL in the mechanism of membrane fission by stimulating Drp1 GTPase activity (Macdonald *et al.*, 2014; Frohman, 2015). Although other distinct mechanisms for mitochondrial fission likely exist, as discussed later, we argue that localized changes in membrane morphology induced by Drp1 at CL- and PE-enriched fluid regions of the MOM facilitate mitochondrial membrane fission.

As an equally plausible alternative scenario, we consider the possibility that the Drp1-induced clustering of CL into nanoscopic membrane domains, which coalesce to stabilize regions of high spontaneous negative membrane curvature, aids and augments the GTP-driven contractility of the straddled Drp1 helical polymer for membrane fission (Figure 7E; Francy *et al.*, 2015). Our FRET data reveal that Drp1 associates more strongly with, and polymerizes more favorably on, precurved LTs relative to flat liposomes. These data support the notion that membrane-mediated protein–protein interactions in Drp1 are considerably stronger on highly curved membranes than on relatively flat membranes, as for dynamin (Roux *et al.*, 2010; Shlomovitz *et al.*, 2011). Coupled with the lower GTPase activity observed for the tightly wound Drp1 polymer under the diffusion-restricted conditions on LTs, high membrane curvature likely serves to constrain the GTP-driven dynamics of the Drp1 polymer and/or the proposed treadmilling of the helical filament (Mears *et al.*, 2011; Morlot *et al.*, 2012; Shnyrova *et al.*, 2013; Francy *et al.*, 2015) in order to promote membrane fission. Moreover, recent studies suggest that conical lipids (here, CL and DOPE) in flat lipid bilayers induce packing defects similar to that induced by high positive membrane curvature upon sequestration (Vamparys *et al.*, 2013). It is therefore conceivable that Drp1 upon CL sequestration intercalates more efficiently, and possibly differentially, into CL-enriched regions of the membrane to generate and stabilize the very narrow membrane tubule diameters required for fission. The observed GTP dependence of the enhanced CL phase transition propensity further suggests that Drp1 sequesters and reorganizes CL primarily through nucleotide-driven conformational rearrangements. These rearrangements presumably function to surmount the high energy barrier that restricts the spontaneous transition of CL-containing membranes from a bilayer to a nonbilayer configuration (Figure 7E). All of

the foregoing scenarios, based on our experimental evidence, potentially explain why the Drp1 polymer discontinuously constricts CL-containing membranes upon GTP hydrolysis toward fission.

Essential Drp1 adaptor proteins such as Mff localize to fission-predisposed, preconstricted mitochondria–ER membrane contact sites, which are generated by the enwrapping of ER-derived membrane tubules and stabilized by the action of actin–myosin cytoskeletal networks that impinge on them (Friedman *et al.*, 2011; Korobova *et al.*, 2013, 2014). Recent evidence points to the existence of cholesterol-containing rafts at these contact sites and the putative localization of Mff in the vicinity (Arasaki *et al.*, 2015). It is therefore conceivable that native CL, enriched at contact sites by virtue of its conical shape and propensity for negative membrane curvature, colocalizes with Mff to recruit Drp1 cooperatively to these regions. Subsequent CL reorganization by Drp1 as a function of its GTP hydrolysis cycle and coordinated regulation by membrane adaptors possibly restrict mitochondrial membrane fission to these contact sites. The coexistence of CL-enriched MIM–MOM contact sites at these locations could further assist in the concerted fission of the mitochondrial double membrane toward achieving complete mitochondrial division.

Under our in vitro experimental conditions, Drp1, unlike dynamin (Morlot *et al.*, 2012; Shnyrova *et al.*, 2013), did not mediate membrane fission. However, unlike dynamin, Drp1 requires interactions with membrane-integrated adaptor proteins (e.g., Mff and MiD49/51) for its participation in membrane fission (Loson *et al.*, 2013; Richter *et al.*, 2015). Although our experiments do not directly address this issue, the absence of membrane fission under our in vitro conditions nevertheless reflects the requirement of membrane adaptors, and possibly membrane tension brought about by the action of the actin-myosin cytoskeleton, in the mechanism of membrane fission. The role of adaptor proteins and membrane tension in Drp1-catalyzed membrane fission awaits further examination.

MATERIALS AND METHODS

Drp1 preparation and fluorescence labeling

Recombinant human Drp1 WT (isoform 3) and mutants were expressed in *Escherichia coli*, purified, and labeled with the fluorescent dye BODIPY-FL using protocols exactly as described previously (Macdonald *et al.*, 2014).

Liposome, GUV, and LT preparation

All lipids, with the exception of NBD-DHPE (Life Technologies, Eugene, OR), were purchased from Avanti Polar Lipids (Alabaster, AL). Liposomes were prepared by extrusion through polycarbonate membranes of 400-nm pore diameter, unless specified otherwise. GUVs were prepared by electroformation as described previously (Macdonald *et al.*, 2014). TMCL- and DPPC-containing lipid mixtures were extruded or electroformed at a temperature >45°C (~55–65°C for DPPC) to accommodate higher melting temperature of the saturated lipids. MOM-like liposomes (MOM-mix) corresponding to outer membrane composition liposomes as reported in Lackner *et al.* (2009) contained 47 mol% DOPC, 25 mol% DOPE, 19 mol% bovine liver phosphatidylinositol (PI), 4 mol% dioleoylphosphatidic acid, 3 mol% bovine heart CL, and 2 mol% DOPS. In MOM-like liposomes containing 10 mol% CL, the mole fraction of PI was correspondingly reduced to 12 mol% in order to maintain negative charge density equivalence. Raft-forming lipid mixtures contained 37.5 mol% DPPC and 25 mol% cholesterol in addition to ~27 mol% DOPC and 10 mol% native CL. The mole fraction of DOPC was increased correspondingly in control liposomes lacking DPPC. Similarly, lipid mixtures containing POPC and cholesterol included 25 mol% POPC, 20 mol% cholesterol, and 25 mol% DOPE, with CL (5–25 mol%) and DOPC (25–5 mol%) making up the remainder. Cholesterol-free control liposomes in this case contained 45 mol% POPC instead. Fluorescently labeled lipids used in this study, Rh-DOPE (C18:1; 1 mol% in liposomes; 0.1 mol% in GUVs), TopFluor-CL (C18:1; 1 mol% in liposomes and GUVs), NBD-DOPE (C18:1; 0.2 mol% in liposomes), and NBD-DHPE (C16:0; 0.5 mol% in GUVs), replaced an equivalent mole fraction of PC or CL (in the case of TopFluor-CL) in the pertinent lipid mixtures. LTs containing 40 mol% C24:1 β-D-galactosylceramide, 35 mol% DOPE, and 25 mol% of either native CL or TMCL were generated by sonication as detailed previously (Leonard *et al.*, 2005). Briefly, the dried lipid mixture was rehydrated in buffer containing 20 mM 4-(2-hydroxyethyl)-1-piperazineethanesulfonic acid (HEPES), pH 7.5, and 150 mM KCl, and sonicated for ~2 min in an Avanti bath sonicator. The final total lipid concentration was 1 mM. The inclusion of very long chain, asymmetric C24:1 β-D-galactosylceramide at ≥40 mol% in the lipid mixture allows for the spontaneous formation of LTs (Stowell *et al.*, 1999; Pinto *et al.*, 2008).

GTPase and velocity sedimentation assays

The stimulated GTPase activity of Drp1 preassembled on liposomes was measured at 37°C using a malachite green–based colorimetric assay as described previously (Macdonald *et al.*, 2014). The final Drp1 and total lipid concentrations were 0.5 and 150 μM, respectively. Nucleotide-dependent sedimentation analyses of Drp1 WT and mutants were performed also as previously described (Macdonald *et al.*, 2014), using 5 μM Drp1 and 1 mM nucleotide final.

Fluorescence spectroscopy

All measurements were made at 25°C. The kinetics of BODIPY-FL–RhPE FRET were measured using a Fluorolog 3-22 spectrofluorometer (Horiba Scientific, Edison, NJ) equipped with an SFA-20 Rapid Kinetics Stopped-Flow Accessory (Hi-Tech Scientific, Bradford-on-Avon, United Kingdom). BODIPY-FL was excited at 470 nm, and the FRET-sensitized emission of rhodamine was monitored at 590 nm. The apparent rate constants for Drp1-membrane binding were obtained by individually fitting each kinetic time trace to a biexponential curve as described previously (Mehrotra *et al.*, 2014). Only the high-amplitude, faster component (k_1) is shown for comparison. The extent of emission intensity change in TopFluor-CL and NBD-DOPE, respectively, upon Drp1 association with liposomes, with or without nucleotide, was monitored using a Tecan Infinite M1000 PRO microplate reader and a SX20 stopped-flow spectrometer (Applied Photophysics, Surrey, United Kingdom), respectively. TopFluor-CL was excited at 470 nm, and emission was monitored at 510 nm. NBD was excited at 455 nm, and emission was monitored using a 488-nm EdgeBasic long-pass edge filter (Semrock, Rochester, NY). The assay buffer (20 mM HEPES, pH 7.5, 150 mM KCl) in each case contained 1 mM dithiothreitol (DTT) and 2 mM $MgCl_2$, except for the cardiolipin titration measurements in Figure 2F, which did not include $MgCl_2$. The presence of Mg^{2+} ions in the assay buffer considerably reduced the extent of Drp1 binding to CL-containing liposomes because of the divalent cation's affinity for the CL head group. For TopFluor-CL steady-state emission intensity measurements, the final protein and total lipid concentrations were 0.5 and 150 μM, respectively. For both steady-state and stopped-flow kinetics fluorescence measurements, the final Drp1 and total lipid concentrations were 0.1 μM and 10, respectively, for BODIPY-FL-Drp1 to Rh-DOPE FRET and 0.5 and 50 μM, respectively, for the NBD-detected CL phase transition. The final concentration of nucleotides in all experiments was 1 mM. In control experiments demonstrating

Ca^{2+}-induced phase transition in CL-containing membrane bilayers, $CaCl_2$ was present at 5–25 mM final.

GUV imaging by confocal fluorescence microscopy

All experiments were conducted at room temperature in assay buffer (20 mM HEPES, pH 7.5, 150 mM KCl) containing 1 mM DTT and 2 mM $MgCl_2$. Images were captured using an Olympus FV1000 IX81 confocal microscope (Olympus USA, Melville, NY) and a 60× oil-immersion objective as described previously (Macdonald *et al.*, 2014). In pertinent experiments, BODIPY-FL–labeled Drp1 was mixed in a 2:3 M ratio with unlabeled Drp1 before addition to GUV-containing chambers. Whenever present, nucleotides (1 mM final) were added to, and equilibrated in, the GUV chambers before Drp1 addition. TopFluor, a BODIPY derivative, was imaged upon excitation using the 488-nm laser line, as was BODIPY-FL-Drp1. In each individual experiment (n = 3), the effect of Drp1 on >25 GUVs was recorded. Unless noted otherwise, the final concentration of Drp1 was 0.5 µM.

Time-lapse EM

Liposomes containing 25 mol% native CL or TMCL, 35 mol% DOPE, and 40 mol% DOPC were prepared by extrusion through polycarbonate membranes of 400-nm pore diameter as described previously (Leonard *et al.*, 2005). Drp1 (2 µM final) was preincubated with liposomes (50 µM total lipid) in buffer containing 20 mM HEPES, pH 7.5, 150 mM KCl, and 1 mM DTT for at least 30 min at room temperature before the initiation of stimulated GTP hydrolysis through the simultaneous addition of $MgCl_2$ (0.5 mM final) and GTP (1 mM final). At specified time points, samples were adsorbed onto carbon-coated grids and stained with 2% uranyl acetate. Images were acquired as described previously (Francy *et al.*, 2015).

Cell culture, immunolabeling, and Western blotting

Mitochondrial morphology and distribution in transfected Drp1-KO mouse embryonic fibroblasts expressing either Drp1 WT or Drp1 4KA were analyzed as previously described (Macdonald *et al.*, 2014). Drp1 expression levels were detected and compared using Western blotting as previously (Macdonald *et al.*, 2014).

ACKNOWLEDGMENTS

An American Heart Association Beginning Grant-in-Aid (13BGIA14810010) awarded to R.R. funded this study. J.A.M. is supported by an American Heart Association Scientist Development Grant (12SDG9130039), X.Q. is supported by a National Institutes of Health grant (R01 NS088192), and C.A.F. is supported by a National Institutes of Health training grant (2T32GM008803-11A1). We thank Patrick van der Wel and Abhishek Mandal (both of the University of Pittsburgh, Pittsburgh, PA) for stimulating discussions on CL and membrane phase behavior.

REFERENCES

Arasaki K, Shimizu H, Mogari H, Nishida N, Hirota N, Furuno A, Kudo Y, Baba M, Baba N, Cheng J, *et al.* (2015). A role for the ancient SNARE syntaxin 17 in regulating mitochondrial division. Dev Cell 32, 304–317.

Ardail D, Privat JP, Egret-Charlier M, Levrat C, Lerme F, Louisot P (1990). Mitochondrial contact sites. Lipid composition and dynamics. J Biol Chem 265, 18797–18802.

Baile MG, Lu YW, Claypool SM (2014). The topology and regulation of cardiolipin biosynthesis and remodeling in yeast. Chem Phys Lipids 179, 25–31.

Ban T, Heymann JA, Song Z, Hinshaw JE, Chan DC (2010). OPA1 disease alleles causing dominant optic atrophy have defects in cardiolipin-stimulated GTP hydrolysis and membrane tubulation. Hum Mol Genet 19, 2113–2122.

Beales PA, Bergstrom CL, Geerts N, Groves JT, Vanderlick TK (2011). Single vesicle observations of the cardiolipin-cytochrome C interaction: induction of membrane morphology changes. Langmuir 27, 6107–6115.

Bethoney KA, King MC, Hinshaw JE, Ostap EM, Lemmon MA (2009). A possible effector role for the pleckstrin homology (PH) domain of dynamin. Proc Natl Acad Sci USA 106, 13359–13364.

Boscia AL, Treece BW, Mohammadyani D, Klein-Seetharaman J, Braun AR, Wassenaar TA, Klosgen B, Tristram-Nagle S (2014). X-ray structure, thermodynamics, elastic properties and MD simulations of cardiolipin/dimyristoylphosphatidylcholine mixed membranes. Chem Phys Lipids 178, 1–10.

Bui HT, Shaw JM (2013). Dynamin assembly strategies and adaptor proteins in mitochondrial fission. Curr Biol 23, R891–R899.

Bustillo-Zabalbeitia I, Montessuit S, Raemy E, Basanez G, Terrones O, Martinou JC (2014). Specific interaction with cardiolipin triggers functional activation of dynamin-related protein 1. PLoS One 9, e102738.

Chan DC (2012). Fusion and fission: interlinked processes critical for mitochondrial health. Annu Rev Genet 46, 265–287.

Chernomordik LV, Kozlov MM (2008). Mechanics of membrane fusion. Nat Struct Mol Biol 15, 675–683.

Ciarlo L, Manganelli V, Garofalo T, Matarrese P, Tinari A, Misasi R, Malorni W, Sorice M (2010). Association of fission proteins with mitochondrial raft-like domains. Cell Death Differ 17, 1047–1058.

Cosentino K, Garcia-Saez AJ (2014). Mitochondrial alterations in apoptosis. Chem Phys Lipids 181, 62–75.

de Almeida RF, Fedorov A, Prieto M (2003). Sphingomyelin/phosphatidylcholine/cholesterol phase diagram: boundaries and composition of lipid rafts. Biophys J 85, 2406–2416.

de Kruijff B, Cullis PR (1980). Cytochrome c specifically induces non-bilayer structures in cardiolipin-containing model membranes. Biochim Biophys Acta 602, 477–490.

DeVay RM, Dominguez-Ramirez L, Lackner LL, Hoppins S, Stahlberg H, Nunnari J (2009). Coassembly of Mgm1 isoforms requires cardiolipin and mediates mitochondrial inner membrane fusion. J Cell Biol 186, 793–803.

Doan T, Coleman J, Marquis KA, Meeske AJ, Burton BM, Karatekin E, Rudner DZ (2013). FisB mediates membrane fission during sporulation in Bacillus subtilis. Genes Dev 27, 322–334.

Francy CA, Alvarez FJ, Zhou L, Ramachandran R, Mears JA (2015). The mechanoenzymatic core of dynamin-related protein 1 comprises the minimal machinery required for membrane constriction. J Biol Chem 290, 11692–11703.

Friedman JR, Lackner LL, West M, DiBenedetto JR, Nunnari J, Voeltz GK (2011). ER tubules mark sites of mitochondrial division. Science 334, 358–362.

Frohlich C, Grabiger S, Schwefel D, Faelber K, Rosenbaum E, Mears J, Rocks O, Daumke O (2013). Structural insights into oligomerization and mitochondrial remodelling of dynamin 1-like protein. EMBO J 32, 1280–1292.

Frohman MA (2015). Role of mitochondrial lipids in guiding fission and fusion. J Mol Med (Berl) 93, 263–269.

Gohil VM, Thompson MN, Greenberg ML (2005). Synthetic lethal interaction of the mitochondrial phosphatidylethanolamine and cardiolipin biosynthetic pathways in Saccharomyces cerevisiae. J Biol Chem 280, 35410–35416.

Hayashi T, Fujimoto M (2010). Detergent-resistant microdomains determine the localization of sigma-1 receptors to the endoplasmic reticulum-mitochondria junction. Mol Pharmacol 77, 517–528.

Heymann JA, Hinshaw JE (2009). Dynamins at a glance. J Cell Sci 122, 3427–3431.

Hong K, Baldwin PA, Allen TM, Papahadjopoulos D (1988). Fluorometric detection of the bilayer-to-hexagonal phase transition in liposomes. Biochemistry 27, 3947–3955.

Horvath SE, Daum G (2013). Lipids of mitochondria. Prog Lipid Res 52, 590–614.

Huang KC, Ramamurthi KS (2010). Macromolecules that prefer their membranes curvy. Mol Microbiol 76, 822–832.

Koirala S, Guo Q, Kalia R, Bui HT, Eckert DM, Frost A, Shaw JM (2013). Interchangeable adaptors regulate mitochondrial dynamin assembly for membrane scission. Proc Natl Acad Sci USA 110, E1342–E1351.

Korobova F, Gauvin TJ, Higgs HN (2014). A role for myosin II in mammalian mitochondrial fission. Curr Biol 24, 409–414.

Korobova F, Ramabhadran V, Higgs HN (2013). An actin-dependent step in mitochondrial fission mediated by the ER-associated formin INF2. Science 339, 464–467.

Labbe K, Murley A, Nunnari J (2014). Determinants and functions of mitochondrial behavior. Annu Rev Cell Dev Biol 30, 357–391.
Lackner LL, Horner JS, Nunnari J (2009). Mechanistic analysis of a dynamin effector. Science 325, 874–877.
Leonard M, Song BD, Ramachandran R, Schmid SL (2005). Robust colorimetric assays for dynamin's basal and stimulated GTPase activities. Methods Enzymol 404, 490–503.
Lewis RN, McElhaney RN (2009). The physicochemical properties of cardiolipin bilayers and cardiolipin-containing lipid membranes. Biochim Biophys Acta 1788, 2069–2079.
Liu J, Kaksonen M, Drubin DG, Oster G (2006). Endocytic vesicle scission by lipid phase boundary forces. Proc Natl Acad Sci USA 103, 10277–10282.
Loson OC, Song Z, Chen H, Chan DC (2013). Fis1, Mff, MiD49, and MiD51 mediate Drp1 recruitment in mitochondrial fission. Mol Biol Cell 24, 659–667.
Macdonald PJ, Stepanyants N, Mehrotra N, Mears JA, Qi X, Sesaki H, Ramachandran R (2014). A dimeric equilibrium intermediate nucleates Drp1 reassembly on mitochondrial membranes for fission. Mol Biol Cell 25, 1905–1915.
Maniti O, Cheniour M, Lecompte MF, Marcillat O, Buchet R, Vial C, Granjon T (2011). Acyl chain composition determines cardiolipin clustering induced by mitochondrial creatine kinase binding to monolayers. Biochim Biophys Acta 1808, 1129–1139.
Marks B, Stowell MH, Vallis Y, Mills IG, Gibson A, Hopkins CR, McMahon HT (2001). GTPase activity of dynamin and resulting conformation change are essential for endocytosis. Nature 410, 231–235.
Marsh D (2009). Cholesterol-induced fluid membrane domains: a compendium of lipid-raft ternary phase diagrams. Biochim Biophys Acta 1788, 2114–2123.
Mears JA, Lackner LL, Fang S, Ingerman E, Nunnari J, Hinshaw JE (2011). Conformational changes in Dnm1 support a contractile mechanism for mitochondrial fission. Nat Struct Mol Biol 18, 20–26.
Mehrotra N, Nichols J, Ramachandran R (2014). Alternate pleckstrin homology domain orientations regulate dynamin-catalyzed membrane fission. Mol Biol Cell 25, 879–890.
Montessuit S, Somasekharan SP, Terrones O, Lucken-Ardjomande S, Herzig S, Schwarzenbacher R, Manstein DJ, Bossy-Wetzel E, Basanez G, Meda P, Martinou JC (2010). Membrane remodeling induced by the dynamin-related protein Drp1 stimulates Bax oligomerization. Cell 142, 889–901.
Morlot S, Galli V, Klein M, Chiaruttini N, Manzi J, Humbert F, Dinis L, Lenz M, Cappello G, Roux A (2012). Membrane shape at the edge of the dynamin helix sets location and duration of the fission reaction. Cell 151, 619–629.
Naylor K, Ingerman E, Okreglak V, Marino M, Hinshaw JE, Nunnari J (2006). Mdv1 interacts with assembled dnm1 to promote mitochondrial division. J Biol Chem 281, 2177–2183.
Ortiz A, Killian JA, Verkleij AJ, Wilschut J (1999). Membrane fusion and the lamellar-to-inverted-hexagonal phase transition in cardiolipin vesicle systems induced by divalent cations. Biophys J 77, 2003–2014.
Pan R, Jones AD, Hu J (2014). Cardiolipin-mediated mitochondrial dynamics and stress response in Arabidopsis. Plant Cell 26, 391–409.
Pinto SN, Silva LC, de Almeida RF, Prieto M (2008). Membrane domain formation, interdigitation, and morphological alterations induced by the very long chain asymmetric C24:1 ceramide. Biophys J 95, 2867–2879.
Praefcke GJ, McMahon HT (2004). The dynamin superfamily: universal membrane tubulation and fission molecules? Nat Rev Mol Cell Biol 5, 133–147.
Renner LD, Weibel DB (2011). Cardiolipin microdomains localize to negatively curved regions of Escherichia coli membranes. Proc Natl Acad Sci USA 108, 6264–6269.
Richter V, Singh AP, Kvansakul M, Ryan MT, Osellame LD (2015). Splitting up the powerhouse: structural insights into the mechanism of mitochondrial fission. Cell Mol Life Sci (*in press*).
Roux A, Koster G, Lenz M, Sorre B, Manneville JB, Nassoy P, Bassereau P (2010). Membrane curvature controls dynamin polymerization. Proc Natl Acad Sci USA 107, 4141–4146.
Sankaram MB, Powell GL, Marsh D (1989). Effect of acyl chain composition on salt-induced lamellar to inverted hexagonal phase transitions in cardiolipin. Biochim Biophys Acta 980, 389–392.
Schlame M, Rabe H, Rustow B, Kunze D (1988). Molecular species of mitochondrial phosphatidylcholine in rat liver and lung. Biochim Biophys Acta 958, 493–496.
Schlame M, Ren M (2006). Barth syndrome, a human disorder of cardiolipin metabolism. FEBS Lett 580, 5450–5455.
Schlame M, Ren M, Xu Y, Greenberg ML, Haller I (2005). Molecular symmetry in mitochondrial cardiolipins. Chem Phys Lipids 138, 38–49.
Schlame M, Towbin JA, Heerdt PM, Jehle R, DiMauro S, Blanck TJ (2002). Deficiency of tetralinoleoyl-cardiolipin in Barth syndrome. Ann Neurol 51, 634–637.
Seddon JM (1990). Structure of the inverted hexagonal (HII) phase, and non-lamellar phase transitions of lipids. Biochim Biophys Acta 1031, 1–69.
Shlomovitz R, Gov NS, Roux A (2011). Membrane-mediated interactions and the dynamics of dynamin oligomers on membrane tubes. New J Phys 13, 065008.
Shnyrova AV, Bashkirov PV, Akimov SA, Pucadyil TJ, Zimmerberg J, Schmid SL, Frolov VA (2013). Geometric catalysis of membrane fission driven by flexible dynamin rings. Science 339, 1433–1436.
Song BD, Leonard M, Schmid SL (2004). Dynamin GTPase domain mutants that differentially affect GTP binding, GTP hydrolysis, and clathrin-mediated endocytosis. J Biol Chem 279, 40431–40436.
Sorice M, Manganelli V, Matarrese P, Tinari A, Misasi R, Malorni W, Garofalo T (2009). Cardiolipin-enriched raft-like microdomains are essential activating platforms for apoptotic signals on mitochondria. FEBS Lett 583, 2447–2450.
Sorice M, Mattei V, Matarrese P, Garofalo T, Tinari A, Gambardella L, Ciarlo L, Manganelli V, Tasciotti V, Misasi R, Malorni W (2012). Dynamics of mitochondrial raft-like microdomains in cell life and death. Commun Integr Biol 5, 217–219.
Stowell MH, Marks B, Wigge P, McMahon HT (1999). Nucleotide-dependent conformational changes in dynamin: evidence for a mechanochemical molecular spring. Nat Cell Biol 1, 27–32.
Strack S, Cribbs JT (2012). Allosteric modulation of Drp1 mechanoenzyme assembly and mitochondrial fission by the variable domain. J Biol Chem 287, 10990–11001.
Tarahovsky YS, Arsenault AL, MacDonald RC, McIntosh TJ, Epand RM (2000). Electrostatic control of phospholipid polymorphism. Biophys J 79, 3193–3200.
Trusova VM, Gorbenko GP, Molotkovsky JG, Kinnunen PK (2010). Cytochrome c-lipid interactions: new insights from resonance energy transfer. Biophys J 99, 1754–1763.
Ugarte-Uribe B, Muller HM, Otsuki M, Nickel W, Garcia-Saez AJ (2014). Dynamin-related protein 1 (Drp1) promotes structural intermediates of membrane division. J Biol Chem 289, 30645–30656.
Vamparys L, Gautier R, Vanni S, Bennett WF, Tieleman DP, Antonny B, Etchebest C, Fuchs PF (2013). Conical lipids in flat bilayers induce packing defects similar to that induced by positive curvature. Biophys J 104, 585–593.
van Meer G, Voelker DR, Feigenson EGW (2008). Membrane lipids: where they are and how they behave. Nat Rev Mol Cell Biol 9, 112–124.
Veatch SL, Keller SL (2003). Separation of liquid phases in giant vesicles of ternary mixtures of phospholipids and cholesterol. Biophys J 85, 3074–3083.
Warnock DE, Hinshaw JE, Schmid SL (1996). Dynamin self-assembly stimulates its GTPase activity. J Biol Chem 271, 22310–22314.
Xu Y, Schlame M (2014). The turnover of glycerol and acyl moieties of cardiolipin. Chem Phys Lipids 179, 17–24.
Zhao H, Michelot A, Koskela EV, Tkach V, Stamou D, Drubin DG, Lappalainen P (2013). Membrane-sculpting BAR domains generate stable lipid microdomains. Cell Rep 4, 1213–1223.